International Journal of Researches on Civil Engineering with Artificial Intelligence

www.ceai.reapress.com

Int. J. Res. Civ. Eng. AI. Vol. 2, No. 4 (2025) 260–287.

Paper Type: Original Article

Optimizing Concrete Compressive Strength Prediction: Artificial Neural Networks Applied to Early and Long-Term Strength Metrics

Elmira Khaksar Njafi[1,*], Hamidreza Rabiefar[2]

[1] Department of Civil Engineering, James Watt School of Engineering, University of Glasgow, United Kingdom; elmira.khaksarnajafi@glasgow.ac.uk.
[2] Department of Civil Engineering, Islamic Azad University, Tehran South Branch, Tehran, Iran; hr_rabiee@azad.ac.ir.

Citation:

Received: 22 December 2024 *Revised: 07 March 2025* *Accepted: 19 June 2025*	Khaksar Njafi, E., & Rabiefar, H. (2025). Optimizing concrete compressive strength prediction: Artificial neural networks applied to early and long-term strength metrics. *International journal of researches on civil engineering with artificial intelligence*, 2(4), 260-287.

Abstract

The study focuses on predicting the 28-day compressive strength of ordinary concrete based on 7-day strength using Artificial Neural Networks (ANNs). As a critical material in construction, accurately forecasting concrete's compressive strength is essential for effective planning and quality control. Traditional methods, including linear regression, have limitations in capturing the nonlinear relationships between mix variables and resulting strength. By utilizing ANNs, which excel in identifying complex patterns, this research proposes a reliable model for compressive strength prediction. Experiments involved testing twelve concrete mix designs with a fixed 10% micro-silica replacement for cement. Each sample's slump (workability) and compressive strength at 7 and 28 days were recorded, with data processed for ANN. The model achieved high accuracy, with a correlation coefficient (R) 0.99 between predicted and actual 28-day strength values. Micro-silica enhanced early and long-term strength, with mixes achieving up to 44.5 MPa at 28 days. Linear regression analysis also yielded robust predictions (R^2=0.958), underscoring the viability of statistical methods alongside ANNs. The ANN model enables early strength estimation, assisting construction decision-making and optimizing resource use. The findings support ANN and micro-silica integration for robust, high-performance concrete. This approach aligns with advancements in AI-driven construction practices, offering a practical tool for early-stage strength prediction and quality assurance in concrete applications.

Keywords: Artificial neural networks, Compressive strength, Concrete mix design, Micro-silica addition, Strength prediction model, Construction quality control.

1 | Introduction

An innovative high-performance concrete called Self-Compacting Concrete (SCC) can fill the formwork evenly without external vibrations and compact and flow under its weight without big components migrating

Corresponding Author: elmira.khaksarnajafi@glasgow.ac.uk
https://doi.org/10.48314/ijrceai.v2i4.71
Licensee System Analytics. This article is an open-access article distributed under the terms and conditions of the Creative Commons Attribution (CC BY) license (http://creativecommons.org/licenses/by/4.0).

or separating, even when reinforced with a lot of material [1], [2]. Researchers have described SCC as a concrete that meets the parameters for flowability, passing ability, and segregation resistance [3], [4]. Further development of SCC has been achieved over the last 20 years using a range of Supplementary Cementitious Materials (SCMs), such as Fly Ash (FA) [5] and Silica Fume (SF) [6]. Several SCMs may substantially affect the fresh and hardened phases of concrete [6]. Particle size is comparable to or smaller than that of Portland Cement (PC), and all SCMs are pozzolanic, meaning involvement in hydration processes occurs. Reactive silica (SiO_2) Pozzolans are not very useful as a cementitious agent when used alone. The cement composite may synergistically overcome the difficulties of employing a single mineral addition using a secondary mineral admixture. A mixture of low-reactive and high-reactive pozzolan is often employed in ternary blended cement concretes to enhance rheological characteristics, pore structure, sulfate and chloride ion infiltration resistance, and high early age strength [7], [8]. Furthermore, nanoparticle incorporation helps improve micropore architecture. Substituting additives for some of the cement in concrete has several benefits, including reducing the material's permeability, increasing its corrosion resistance, and strengthening it in both bending and compressive tests. The pozzolanic interaction between these particles and $Ca(OH)_2$ in cement and their tiny particle size and high-water absorption capacity (a consequence of their dry surface saturation) contribute to these advantages. The effects of nano-silica on microstructures and hydration in concrete specimens were studied by Wang et al. [9], who demonstrated that these materials improve hydration, microscopic morphology, and compressive strength. According to research by Assaedi et al. [10], calcium silicate gel and hydrated calcium aluminosilicate are crucial for improving microstructure and enhancing compressive strength when combining nano-silica with concrete. According to Louis's research [11], silica sand increases compressive strength. In addition, Abd El-Baky et al. [12] found that the specimens' compressive strength increased by 55.7% and their bending strength by 46.9% when silica sand was used in place of some cement. However, this method reduced the concrete paste's workability. Various factors, including the chemical composition of the sand, particle size, mixing conditions, specimen age, and type of cement, determine the optimal percentage of silica sand in the concrete mix design. For instance, according to research by Chaudhary et al. [13], the maximum compressive and tensile strengths could be achieved with 6% and 3% silica sand, respectively. However, using up to 15% of silica sand instead of cement is permissible. Several sectors have seen a dramatic increase in productivity and innovation due to merging AI with manufacturing, which has also rethought the assumptions behind more conventional methods [14–17]. With the help of Artificial Intelligence (AI), some sectors have rethought their capabilities. When it comes to optimizing productivity, minimizing mistakes, and ensuring uniform quality throughout the whole manufacturing process with AI, the mechanical sector has seen tremendous progress thanks to complete end-to-end automation [18]. Due to its many complicated obstacles, the building sector cannot innovate [19]. In terms of innovation and output, the construction industry is far behind other sectors [20–22]. For decades, it has stuck to tried-and-true building methods [23]. Because this sector accounts for 12% of the world GDP, it is critical to invest in R&D, new ideas, and real-world applications [24]. Much research is happening in the construction business, but much of it is focused on improving materials, optimizing designs, studying structural behavior, etc. [25]. Even though there are many new types of concrete on the market that aim to solve specific problems, the construction industry as a whole continues to face issues like post-construction waste [26], insufficient sustainability [27] and flexibility [28], lengthy construction times [29], and expensive materials [30]. More automated and optimal ways must be used in the building processes [31] Chui, 2019 #6044}. By offering a solution to the problems listed above, additive manufacturing has started a new era in the building sector [32]. Artificial Neural Networks (ANNs) are particularly well-suited for predicting the compressive strength of concrete due to their capability to model complex, nonlinear relationships among multiple variables without the need for predefined equations. Unlike traditional regression methods, ANNs can process large datasets and identify hidden patterns essential for accurate predictions in systems with intricate, interdependent factors, such as the components of concrete mix designs. This study introduces the novel approach of using micro-silica, a highly reactive pozzolan, as a variable within the ANN model. Including micro-silica improves the model's predictive capability and provides insights into its effects on strength development. This approach allows the ANN to capture both the nonlinear behavior of the concrete and the added benefits of micro-silica, leading to a more precise estimation of long-term compressive strength based on early-age data. Concrete is one of the most critical and widely used construction materials worldwide, playing a vital role in infrastructure and urban development. Its extensive use underscores the importance of accurately predicting its performance, particularly its compressive strength, a key indicator of quality and durability. Traditional methods for predicting concrete strength, such as linear and nonlinear regression, often struggle with the complex, nonlinear interactions within concrete's composition. Recent advancements in AI, specifically neural networks, have introduced new possibilities for modeling these intricate relationships. Neural networks, which mimic the structure of the human brain, consist of interconnected neurons that work together to process inputs and yield precise predictions for complex systems. This study leverages neural networks to predict the 28-day compressive strength of concrete based on 7-day strength measurements and mix design variables, including micro-silica addition, to improve accuracy in early-stage construction planning and quality control. This study aims to develop a neural network model capable of reliably forecasting 28-day compressive strength using early-age data and mix components, allowing construction projects to optimize resources and ensure safety. The research involves experimental testing on 12 concrete mix designs, each with a 10% replacement of cement by micro-silica, and records both slump and compressive strength at 7 and 28 days. Statistical analysis using SPSS and neural network modeling via MATLAB's neural net fitting toolbox will facilitate the validation of the model's accuracy. By comparing the neural network's predictions with actual experimental results, this study aims to assess the effectiveness of neural networks as a practical tool in concrete strength prediction, paving the way for their integration into construction industry practices for enhanced efficiency and reliability.

2 | Methodology

2.1 | Materials

This section describes the core materials used in the concrete mix and their contributions to compressive strength, which is essential for understanding the experimental process and interpreting the results [33]. Concrete primarily consists of cement, water, aggregates, and additives, each contributing uniquely to its final properties. Cement serves as the binding material, holding aggregates together and giving the concrete its stone-like rigidity. In this study, hydraulic cement, specifically PC, is used due to its high reactivity with water and compatibility with structural concrete applications. The primary chemical constituents of cement include lime (CaO), silica (SiO_2), alumina (Al_2O_3), iron oxide (Fe_2O_3), magnesium oxide (MgO), sulfur trioxide (SO_3), and alkalis. These compounds play distinct roles: tricalcium silicate (C_3S) and dicalcium silicate (C_2S) are crucial for strength development. C_3S reacts quickly with water, providing early strength and generating significant heat, whereas C_2S reacts more slowly, contributing to long-term strength. This balance of compounds helps achieve both early and sustained compressive strength, with considerations for sulfate resistance provided by specific chemical adjustments in the cement [34]. Water is another critical component, initiating the hydration process that binds cement particles to form the hardened concrete matrix. Water quality significantly impacts the final concrete strength; hence, only water free from harmful impurities (such as excess chlorides, sulfates, and organic matter) is used at acceptable pH levels ranging between 6 and 8 for concrete water to avoid interference with the hydration reaction. Ensuring clean, impurity-free water prevents issues such as delayed setting times, reduced compressive strength, and corrosion of reinforcing steel within the concrete. Aggregates, both coarse and fine, are essential for concrete's structural integrity and strength. Coarse aggregates, generally gravel, provide bulk and stability, while fine aggregates, such as sand, fill voids within the mix, contributing to density and durability. The aggregates used in this study are selected based on shape (preferably rounded or angular), cleanliness, and grading, which influences the workability and strength of the final mix. Proper gradation ensures a dense packing of particles, minimizing voids and thereby enhancing the concrete's compressive strength and overall performance. Additives, specifically SCMs like micro-silica, are incorporated to improve the concrete's performance. Micro-silica, a fine pozzolanic material, reacts with calcium hydroxide in the mix to produce additional Calcium Silicate Hydrate (C-S-H), which strengthens the microstructure of the concrete. This addition enhances compressive strength and improves durability by making the concrete less permeable and more resistant to chemical attacks. Through improved density and microstructure, micro-silica contributes significantly to the durability and long-term strength of the concrete, making it suitable for high-performance applications [34], [35].

2.2 | Experimental Procedure

The concrete mixes in this study were specifically designed by adjusting the proportions of cement, water, coarse and fine aggregates, and micro-silica to study their effect on compressive strength. Each mix incorporated a fixed cement replacement by micro-silica, typically at 10% of the total cement weight, enhancing the concrete's density and overall strength. The remaining cement content constituted approximately 90% of the binder material. Water-to-cement ratios were carefully controlled to optimize workability and hydration, with values typically ranging from 0.4 to 0.5, ensuring sufficient flow while promoting adequate strength development. Coarse and fine aggregates were incorporated to make up around 60-70% of the concrete volume, achieving the necessary bulk and density [36]. The fresh concrete was poured into 15 × 15 ×15 cm cubic molds and compacted to remove air voids that might reduce strength. After casting, samples were demolded and cured in water to ensure consistent hydration across all tests. The curing process was standardized to promote uniform strength gain, which is essential for accurately comparing results. In preparing the concrete samples, the cement, water, aggregates, and micro-silica materials were precisely measured and mixed according to the specified design ratios. Once the mix was thoroughly blended to achieve a homogeneous consistency, and poured into 15x15x15 cm cubic molds. Care was taken to compact the fresh concrete within each mold, essential for eliminating trapped air that could weaken the structure. Compaction was achieved through manual or mechanical vibration to ensure a dense, uniform sample without internal voids, which is crucial for accurate compressive strength testing [37]. After casting, the samples were allowed to set in the molds for 24 hours under controlled conditions. After de-molding, the cubes were transferred to a water-curing tank, where full submersion and curing at a constant temperature were applied to promote consistent hydration and strength development. Water curing is critical in concrete preparation, as it maintains the moisture necessary for the hydration reaction of cement, preventing surface drying and ensuring uniform strength development throughout each sample. Curing was carried out according to standardized conditions, ensuring that all samples reached the specified testing ages—7 and 28 days—under comparable conditions, thus providing reliable and consistent results across all tests. *Fig. 1* illustrates the step-by-step process involved in the preparation and testing of concrete, showcasing each stage from mixing to final assessment.

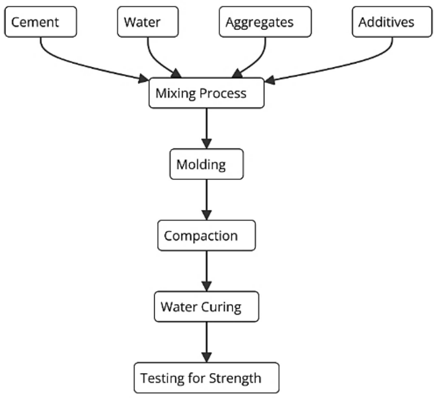

Fig. 1. Concrete preparation and testing process flow.

2.3 | Compressive Strength Test

The slump test is a standardized procedure performed according to ASTM C143 or EN 12350-2 [38] to evaluate the workability and consistency of fresh concrete. This test ensures that the mix achieves the desired flowability, which is essential for proper placement and compaction, especially in situations with dense reinforcement or complex formwork. Workability is a critical factor in concrete performance, influencing its ease of handling, transportation, and final structural quality [36]. Several materials and tools are required to perform the slump test. An Abrams cone is used as the primary mold; this is a truncated metal cone with a height of 30 cm, a bottom diameter of 20 cm, and a top diameter of 10 cm. The cone is placed on a flat, non-absorbent base plate to prevent moisture loss and provide stability during the test. A tamping rod, typically made of metal with a diameter of 16 mm and a length of 60 cm, is used to compact the concrete in each layer. After removing the cone, a measuring scale is also needed to record the slump measurement. The procedure begins by placing the Abrams cone firmly on the base plate. The cone is filled with fresh concrete in three equal layers to ensure consistent density and avoid the formation of air pockets. The first layer fills one-third of the cone's height and is compacted 25 times with the tamping rod. Each tamp is evenly distributed across the layer to ensure uniformity. The second layer is added, filling up to two-thirds of the cone, and is tamped 25 times, with the rod penetrating slightly into the previous layer to improve the bond between layers. The third and final layer fills the cone to the top, and it is tamped 25 times, with the excess concrete struck off level with the cone's rim to ensure a flat surface [37]. After filling and leveling, the cone is carefully lifted vertically to allow the concrete to slump naturally under its weight. This step requires precision, as the cone must be lifted slowly and without any lateral or twisting motion to avoid disturbing the concrete's shape. Once the cone is removed, the distance between the cone's original height and the slumped concrete's highest point is measured with a scale. This measurement, known as the slump, indicates the mix's workability. The slump measurement is recorded in millimeters, and different slump ranges provide insights into the workability and potential applications of the concrete mix. A low slump (0-25 mm) indicates a stiff, low-workability mix suitable for pavements or mass concrete applications where flowability is less critical. A medium slump (50-100 mm) suggests a general-purpose mix suitable for most structural applications, while a high slump (100-175 mm) indicates a highly workable mix that is ideal for areas with dense reinforcement or intricate shapes, where ease of placement is crucial [39]. While the slump test does not require a specific calculation Eq, interpreting the results according to industry standards is essential. The targeted slump value must align with the mix design to ensure the concrete is workable yet dense enough to achieve the desired strength and durability. This controlled workability assessment allows adjustments if needed, ensuring the concrete mix is suitable for the intended application.

2.4 | Data Collection and Preparation

Data collection in this study involved recording measurements from the slump and compressive strength test, which provided essential input parameters for the ANN model. Each concrete sample's slump was measured immediately after mixing to assess workability, while compressive strength data was collected at 7 and 28 days. These data points were critical, representing the concrete's early and standard strengths and enabling the ANN model to learn the relationship between initial mix properties and final strength outcomes [39]. Once collected, the raw data was cleaned to ensure accuracy and consistency. Data cleaning involved identifying and correcting any measurement errors or inconsistencies, such as outliers or incomplete data points, which could skew the ANN's predictions. This step also included verifying that all samples followed the same testing protocols, ensuring uniformity across the dataset. Normalization was performed to prepare the data for input into the ANN. Normalization scales the data to a standard range, typically between 0 and 1 or -1 and 1, depending on the model requirements. This step is crucial because it ensures that each variable contributes proportionately to the ANN model, preventing any feature (such as compressive strength) from dominating due to a larger numerical scale. In addition to normalization, transformation techniques were applied where necessary to improve data distribution and enhance the model's learning efficiency. For instance, data transformations, such as log or square root transformations, were applied to non-linear data distributions to make them more linear, improving the ANN's predictive accuracy [40]. This cleaned, normalized, and transformed dataset was fed into the ANN model. By preparing the data in this structured manner, the ANN could accurately interpret the input variables, allowing it to predict the 28-day compressive strength based on the mix design and early-age strength results with high precision.

2.5 | Artificial Neural Network Model

ANNs are computational models inspired by the brain's structure, allowing advanced machine learning, knowledge representation, and predictive modeling in complex systems. In ANNs, multiple interconnected neurons simulate the processing abilities of the human brain, making these networks well-suited for tasks like pattern recognition, classification, and function approximation [41]. ANNs consist of three main layers: Input layer: Receives raw data inputs. Hidden layers: Process inputs through weighted connections, determining the network's learning power. Output layer: Provides the network's final output based on learned patterns in the data. The neurons in each layer are connected via weights, which adjust during training to minimize prediction errors. The primary aim of training is to optimize these weights, enabling the network to approximate complex functions.

2.5.1 | Mathematical model of neurons

Each neuron computes its output by applying an activation function to the weighted sum of its inputs plus a bias term. The basic equations governing this process are

$$\begin{aligned} n &= W \cdot P + b \\ a_{out} &= f(n) \end{aligned}, \tag{1}$$

where W represents the weight matrix, P is the input vector, b is the bias, $f(n)$ is the activation function applied to the sum n. The activation function can vary based on the application, with commonly used functions being the sigmoid, hyperbolic tangent (tanh), and Rectified Linear Unit (ReLU) functions [42]. For example, the sigmoid function is defined as

$$f_{sig}(n) = \frac{1}{1 + e^{-n}}. \tag{2}$$

The hyperbolic tangent functions as

$$f_{tanh}(n) = \frac{e^{n} - e^{-n}}{e^{n} + e^{-n}}. \tag{3}$$

These functions introduce non-linearity, enabling the network to model complex relationships.

2.5.2 | Types of neural networks

Single-layer perceptron solve linearly separable problems using binary output values. The sign of the weighted input sum determines the output. Multi-Layer Perceptron (MLP) extend this by using multiple layers, enabling them to model non-linear relationships. MLP with a Backpropagation network includes hidden layers, allowing for complex function approximation. The backpropagation algorithm adjusts weights to minimize error by calculating the gradient of the error function concerning each weight. For backpropagation, the error at each output neuron is

$$e_n = t_n - a_n, \tag{4}$$

where t_n is the target output, and a_n is the actual output. The overall network error can be defined as [43]

$$F(K) = \sum_{j=1}^{n} e_j^2. \tag{5}$$

The weight updates during training follow.

$$W_n(K + 1) = W_n(K) - \alpha \cdot \Delta W_n(K), \tag{6}$$

where α is the learning rate, controlling the adjustment magnitude at each step.
3. Radial Basis Function (RBF) Networks: In RBF networks, hidden neurons use a Gaussian activation

function, focusing on localized input patterns. This is useful in classification and clustering tasks where inputs are mapped to outputs based on proximity in feature space, with the Gaussian function

$$f_{RBF}(x) = e^{-\gamma\|x-\mu\|^2}, \quad (7)$$

where μ represents the center of the function, and γ controls the spread, the training process in ANNs aims to minimize the difference between predicted and actual outputs by adjusting weights through backpropagation. This algorithm calculates gradients at each layer, propagating the error backward to optimize the weights. Training can occur via batch learning, where weights update after the entire dataset is processed, or online learning, which adjusts weights after each example, enabling dynamic learning but with increased adjustment variance. The error minimization process in ANN training involves calculating the network's prediction error, which is the difference between the network's output and the target output. This error is quantified using the Eq $F(K) = \sum_{j=1}^{n} e_j^2$, where $F(K)$ represents the total error at iteration K, and e_j is the individual error at each output node j. By summing the squared differences across all output nodes, this function provides a clear metric to evaluate how close the network's predictions are to the desired values. Minimizing this error function is a core objective in training, as it directly impacts the network's accuracy and effectiveness in generalizing patterns within the data [43], [44]. The gradient calculation in backpropagation is a critical component of the training process, where gradients are computed for each weight to adjust them in the direction that reduces the error. Precisely, the gradient of the error function for each weight is calculated in a series of steps. First, the error gradient is determined at the output layer and propagated backward through the network to update weights at each preceding layer. For each layer, the weight adjustments are proportional to the partial derivative of the error with respect to each weight, allowing the algorithm to correct the weights to minimize the overall error. By repeating this process across multiple iterations, backpropagation refines the network's internal parameters for improved predictive accuracy. Finally, the training process iterates through this cycle of forward passes, error calculation, and backpropagation until a predefined convergence criterion or an acceptable error threshold is reached. Convergence is achieved when successive iterations result in minimal changes to the error function, indicating that the network has reached an optimal or near-optimal configuration of weights. This convergence criterion ensures that the model has sufficiently learned the data patterns without overfitting, allowing it to generalize effectively on new, unseen data. The training process balances accuracy with efficiency by setting appropriate convergence thresholds, producing a well-trained neural network capable of reliable predictions. *Table 1* illustrates the physical characteristics of the cement consumed, providing a comparative overview of key parameters. *Table 2* illustrates the specifications of the super-lubricant used in the study, detailing its key physical and chemical properties. *Table 3* illustrates the various designs created during this study, providing a detailed comparison of their structural and functional aspects. *Table 4* illustrates important ratios in fabricated designs, showcasing critical metrics used to evaluate the balance and functionality of design structures. *Fig. 2* illustrates the structure of a neural network neuron model, detailing the input through dendrites, weighted summation in the cell body, activation function application, and output via the axon. *Fig. 3* illustrates the structure of a neural network model, including inputs, weights, summation through a transfer function, an activation function, and the resulting output.

Table 1. Physical characteristics of cement consumed.

Cement Type	Specific Gravity (gr/cm^3)	Special Surface (cm^2/gr)	Primary Grip (min)	Final Grip (min)	Expansion (%)
Caspian	3.15	3255	130	192	0.36

Table 2. Specifications of the super-lubricant used.

Specification	Details
Chemical composition	Modified poly acid copolymers
Ionic nature	Anionic
Color	Dark green

Table 2. Continued.

Specification	Details
Physical condition	Liquid
pH	7 ± 1
Specific gravity	1.1 ± 0.02 at 20 °C
Chloride (PPM)	Up to 500

Table 3. Designs made in this study.

Row	Plan Name	Cement (Kg/m³)	Pose and Velan Type	Pose Wolan (Kg/m³)	Gravel (Kg/m³)	Sand (Kg/m³)	Water (Kg/m³)	Sp	w/c	s/c
1	C250	250	---	0	1290	898	100	0.3	0.4	0.1
2	C300	300	---	0	1225	849	120	0.3	0.4	0.1
3	C350	350	---	0	1179	820	140	0.3	0.4	0.1
4	C400	400	---	0	1130	780	160	0.3	0.4	0.1
5	C450	450	---	0	1090	762	180	0.3	0.4	0.1
6	C500	500	---	0	1040	675	200	0.3	0.4	0.1
7	C250S	225	Micro Silica	25	1290	898	100	0.3	0.4	0.1
8	C300S	270	Micro Silica	30	1225	849	120	0.3	0.4	0.1
9	C350S	315	Micro Silica	35	1179	820	140	0.3	0.4	0.1
10	C400S	360	Micro Silica	40	1130	780	160	0.3	0.4	0.1
11	C450S	405	Micro Silica	45	1090	762	180	0.3	0.4	0.1
12	C500S	450	Micro Silica	50	1040	675	200	0.3	0.4	0.1

Table 4. Important ratios in fabricated designs.

Row	Plan Name	Lubricant (%)	Water-to-Powder Ratio	Ratio of Wolan Pose to Cement (Weight %)
1	C250	0.3	0.4	10
2	C300	0.3	0.4	10
3	C350	0.3	0.4	10
4	C400	0.3	0.4	10
5	C450	0.3	0.4	10
6	C500	0.3	0.4	10
7	C250S	0.3	0.4	10
8	C300S	0.3	0.4	10
9	C350S	0.3	0.4	10
10	C400S	0.3	0.4	10
11	C450S	0.3	0.4	10
12	C500S	0.3	0.4	10

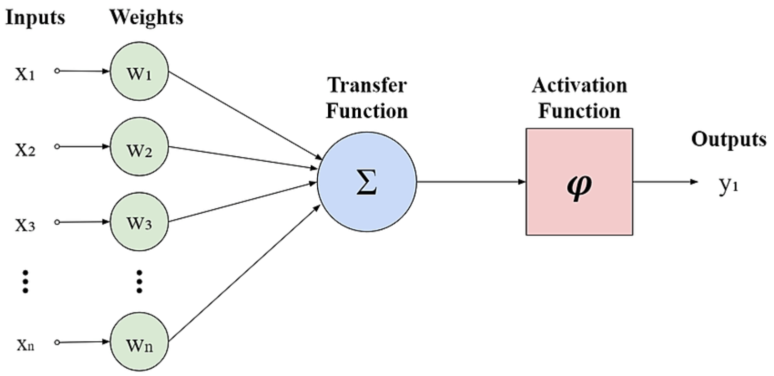

Fig. 2. Diagram of a neural network neuron model, illustrating inputs through dendrites, weighted summation in the cell body, application of an activation function, and output through the axon.

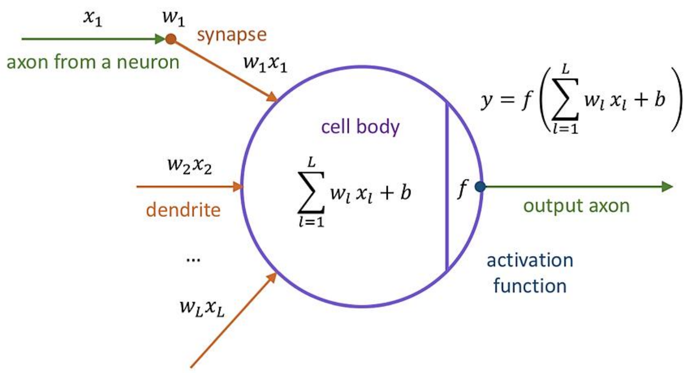

Fig. 3. Neural network model inputs, weights, summation through a transfer function, activation function, and resulting output.

3 | Results and Discussion

3.1 | Objectives and Test Overview

This section outlines the primary objectives and tests conducted in the experimental analysis of the 12 concrete mix designs. The aim was to examine how varying cement content and micro-silica addition influence concrete's workability and compressive strength [45]. The first objective involved evaluating workability through slump tests. The slump test was employed to assess the workability of each mix design. Workability indicates the ease with which concrete can be mixed, placed, and finished, which is vital for ensuring quality and uniformity in construction. By performing slump tests on each mix, the study examined how cement and micro-silica content changes affect the concrete's fluidity and consistency. This assessment was crucial for determining whether higher cement grades or adjustments with micro-silica enhance or reduce the workability of concrete. The second objective assessed strength via compressive strength tests conducted at 7 and 28 days. Compressive strength tests were performed on concrete samples at both 7 and 28 days to evaluate each mix's structural strength. The 7-day test measured early-age strength, which is significant for projects requiring rapid formwork removal or early load application. The 28-day test, on the other hand, measured long-term strength, which is critical for understanding the concrete's ultimate load-bearing capacity. These tests allowed for an evaluation of the impact of different cement grades and the inclusion of micro-silica on both short-term and long-term strength, providing insights into the durability and suitability of each mix design for various structural applications. This study used river sand as the fine aggregate in the concrete mixes. Initial tests indicated that the sand did not fall within the permissible particle size distribution range according to standard requirements. All sand was sieved through sieve no. 4 to address this, and a granulation test was conducted to ensure appropriate grading. The sand had a diameter range of 0.4-75 mm, a specific gravity of 2700 kg/m³ in a saturated state with a dry surface, and a 24-hour water absorption rate of 1.5%.

3.2|Workability Results (Slump Test)

The slump test results offer valuable insights into the workability and fluidity of the twelve distinct concrete mixes, highlighting how variations in cement content and micro-silica addition influence these properties. Workability, assessed through slump values, reflects the ease of placing, compacting, and finishing each mix, which is crucial for construction applications requiring specific flow and placement characteristics [33]. The results in *Table 5* reveal that mixes with higher cement content achieved the highest slump values. For instance, mix C500 and mix C500S, both with 500 kg/m³ of cement, exhibited slump values of 10 cm, indicating a high degree of workability. Similarly, C450 and C450S, with slightly reduced cement content at 450 kg/m³, also showed high slump values of 10 cm and 9 cm, respectively. As cement content decreases, a trend emerges where slump values proportionally decline. For example, the C400 and C400S mixes, each containing 400 kg/m³ of cement, displayed slump values of 9 cm and 7.5 cm. This apparent relationship between increased cement content and greater slump values is likely due to the enhanced paste volume, which improves the concrete's fluidity, making it easier to work with and suitable for placements requiring high workability. The addition of micro-silica also has a measurable impact on the slump, though this effect is marginal. Comparing corresponding mixes with and without micro-silica illustrates this influence. For example, while C500 without micro-silica achieved a 10 cm slump, adding micro-silica in C500S slightly reduced the slump to 10 cm. Similarly, for C400, the slump value was 9 cm without micro-silica, dropping to 7.5 cm when micro-silica was added in C400S. This slight reduction is attributed to micro-silica's high surface area and capacity to absorb free water within the mix, lowering the available water for flow and slightly decreasing the workability. Other mixes, such as C300 and C300S, demonstrated similar behavior with slump values of 7 cm for C300 and 6 cm for C300S. These results underscore a critical balance between workability and the benefits of micro-silica in enhancing strength. While higher cement content reliably improves workability, enhancing the ease of placement and finishing, micro-silica additions provide beneficial strength gains despite their slight impact on slump reduction. The trade-off between workability and strength must be carefully managed in applications where both attributes are essential, as the slump values and strength characteristics in subsequent sections provide a complete picture for selecting concrete mixtures tailored to specific structural requirements. *Fig. 4* illustrates the particle size distribution of sand, showing the percentage passing through a sieve for two sand samples labeled "Rin" and "BII." The curve for "Rin" (blue) consistently shows a higher percentage passing at each particle size, indicating a finer particle distribution compared to "BII" (orange). Both distributions approach 100% passing as particle size increases to 10 mm, with "Rin" achieving near-complete passing at smaller particle sizes than "BII." This difference suggests variations in gradation, which could impact the concrete mix's workability and strength characteristics. *Fig. 5* displays the heights (in cm) of various designs labeled from C300 to C500S. The highest values, at 10 cm, appear in designs C450, C500, and C500S, while the lowest heights, at 6 cm, are found in designs C250S and C300S. Other designs range between 6.5 and 9 cm, with C400S reaching 9 cm and several designs like C300, C350, and C450S falling between 7 and 7.5 cm. This indicates a notable variation in height across different designs.

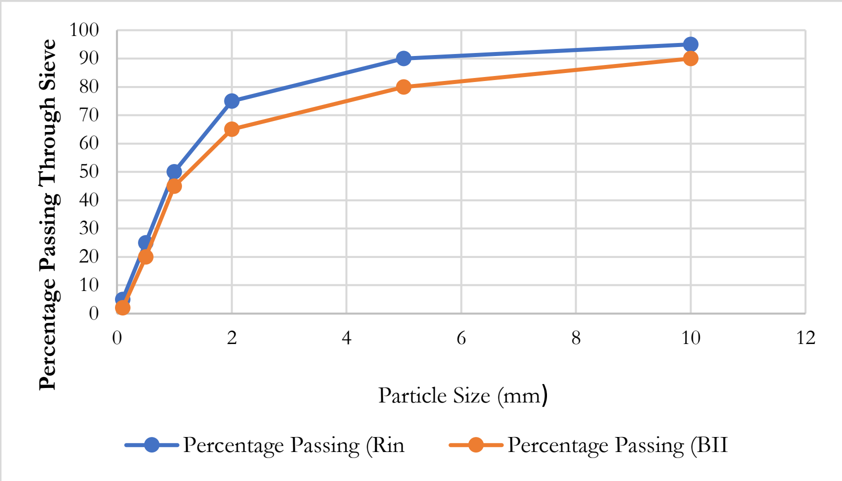

Fig. 4. Graining of the sand used.

Table 5. Results of the slump experiment of 12 fabricated designs.

Row	Plan Name	Slump (cm)
1	C250	6.5
2	C300	7
3	C350	7.5
4	C400	9
5	C450	10
6	C500	10
7	C250S	6
8	C300S	6
9	C350S	7
10	C400S	7.5
11	C450S	9
12	C500S	10

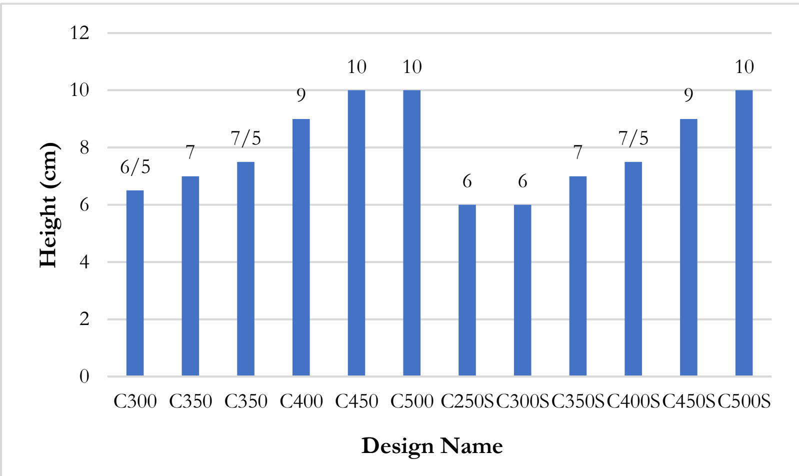

Fig. 5. The results of the slum test for all the designs made.

3.3 | Compressive Strength Results

The compressive strength test results, as presented in *Table 6*, provide valuable insights into the load-bearing capacity and mechanical performance of each concrete mix at both 7 days and 28 days. Evaluating compressive strength at these stages allows us to understand how cement content and micro-silica additions affect the concrete's development over time, which is essential for determining the structural suitability of each mix.

3.3.1 | Compressive strength at 7 days

The 7-day compressive strength results highlight that mixes with higher cement content consistently exhibit increased early-age strength. For instance, concrete mixes with 500 kg/m³ of cement, such as C500 and C500S, achieved strengths of 30 MPa and 33 MPa, respectively. Similarly, mixes containing 450 kg/m³ of cement, like C450 and C450S, attained 29 MPa and 31 MPa compressive strengths. These observations suggest a strong correlation between cement content and early strength, with higher cement mixes demonstrating superior early-age performance, likely due to the increased hydration activity provided by the more significant amount of cementitious material. Additionally, the results reveal that micro-silica inclusion positively influences the early compressive strength. Mixes with micro-silica, such as C500S and C450S, generally displayed slightly higher 7-day strength values than those without micro-silica. For example, C500S reached 33 MPa compared to 30 MPa in C500, while C450S recorded 31 MPa against 29 MPa in C450. This trend is attributed to the fine particle size and pozzolanic reactivity of micro-silica, which enhances particle packing and fills micro-pores within the concrete matrix. By participating in the pozzolanic reaction, micro-silica reacts with calcium hydroxide, creating additional C-S-H that strengthens the concrete's microstructure even at early ages. The 7-day compressive strength results confirm that higher cement content significantly impacts early strength development, with mixes containing more cement achieving more incredible strengths. This finding is particularly beneficial for applications that require early demolding or the early application of loads, as higher cement content accelerates the concrete's strength gain. Additionally, the modest increase in early strength observed in mixes with micro-silica suggests that micro-silica can enhance early-age performance. Micro-silica's ultrafine particles fill voids and improve the packing density within the concrete matrix. At the same time, its reactivity contributes to early strength by forming additional C-S-H gel. These results underscore the advantages of optimizing cement content and micro-silica in concrete mix designs. Structural applications that prioritize early strength, including micro-silica and higher cement content, offer a viable approach to achieving the necessary mechanical properties. This approach ensures that concrete meets strength requirements promptly, supporting efficient construction schedules without compromising the workability and overall performance of the mix.

3.3.2 | Compressive strength at 28 days

The 28-day compressive strength results, as presented in *Table 6*, provide comprehensive data on the long-term mechanical performance of each concrete mix, highlighting the benefits of both high cement content and micro-silica addition in enhancing the concrete's structural integrity. The 28-day compressive strength measurements demonstrate a consistent strength gain across all mixes, with mixes incorporating micro-silica, such as C500S and C450S, achieving the highest compressive strengths. For example, C500S reached a compressive strength of 44.5 MPa, while C450S recorded 42 MPa. This trend suggests that micro-silica contributes to significant strength enhancement over time. Moreover, a clear linear relationship is observed between cement content and 28-day strength, with higher cement levels consistently leading to greater compressive strength. Mixes with higher cement content, like C500 and C500S, achieved compressive strengths of 40 MPa and 44.5 MPa, respectively, while mixes with lower cement content, such as C250 and C250S, showed lower strengths at 23 MPa and 26 MPa. The 28-day compressive strength results confirm the advantageous effects of micro-silica in enhancing long-term concrete strength, especially when combined with higher cement content. Due to its fine particle size and pozzolanic reactivity, micro-silica undergoes a secondary reaction with the calcium hydroxide produced during cement hydration. This reaction generates additional C-S-H, a key component in strengthening the concrete matrix. This process increases compressive strength and reduces porosity by filling voids within the concrete structure, thereby improving the overall durability and impermeability of the concrete. The impact of micro-silica is particularly pronounced in mixes with high cement content, where the additional C-S-H formed from the pozzolanic reaction further refines the pore structure and enhances mechanical performance. As evidenced in *Table 6*, micro-silica mixes consistently outperformed their counterparts without micro-silica, showcasing the potential of micro-silica for producing high-performance concrete that meets rigorous structural demands. These findings support the strategic use of micro-silica in concrete mix designs to achieve superior long-term strength [36]. In applications requiring high durability and load-bearing capacity, including micro-silica with increased cement content is a beneficial approach. This combination optimizes the concrete's compressive strength and structural integrity, ensuring reliable performance over the concrete's lifecycle [46]. *Fig. 6* illustrates the sequence of damage in the material. *Fig. 7* illustrates the 7-day and 28-day compressive strength results (in MPa) for various concrete mix designs. The blue bars represent the 7-day strength, while the orange bars show the 28-day strength. Overall, mixes with higher cement content, such as C450 and C500, exhibit higher early (7-day) and long-term (28-day) strengths. Including micro-silica (indicated by the "S") generally enhances both 7-day and 28-day compressive strengths. For example, C500S achieved the highest 28-day strength of 44.5 MPa, reflecting the positive impact of both high cement content and micro-silica addition on strength development over time. This trend suggests that both cement content and micro-silica inclusion play a crucial role in optimizing early and long-term strength. *Table 7* illustrates the prediction of 28-day compressive strength along with the corresponding error values.

a.

b.

c.

Fig. 6. Sequence of damage in the material; a. Initial crack formation, b. Progression of damage, c. Severe material deformation.

Table 6. Compressive strength 7 and 28 days of 15 cm cube samples for 12 mixing designs.

Row	Plan Name	7-Day Compressive Strength (MPa)	28-Day Compressive Strength (MPa)
1	C250	10.5	23
2	C300	18	28
3	C350	20.5	33.5
4	C400	27	37
5	C450	29	38
6	C500	30	40
7	C250S	13.5	26
8	C300S	19	34
9	C350S	21	35.5
10	C400S	30	41
11	C450S	31	42
12	C500S	33	44.5

Table 7. Predicting 28-day compressive strength and error values.

Plan Name	Lab Results (MPa)	Results Linear Regression (MPa)	Error Linear Regression (%)	Results Neural Network (MPa)	Error Neural Network (%)
C250	23	23.84	3.64	23.70	3.04
C300	28	29.55	5.55	27.19	2.91
C350	33.5	31.83	5.00	33.05	1.34
C400	37	36.86	0.39	37.32	0.88
C450	38	38.78	2.06	37.75	0.65
C500	40	40.02	0.05	38.22	4.44
C250S	26	27.45	5.59	27.17	4.49
C300S	34	32.10	5.58	33.25	2.20
C350S	35.5	34.34	3.26	35.68	0.51
C400S	41	41.40	0.98	39.23	4.32
C450S	42	42.95	2.26	41.96	0.10
C500S	44.5	45.19	1.55	44.52	0.04
∑	-	-	2.99	-	2.08

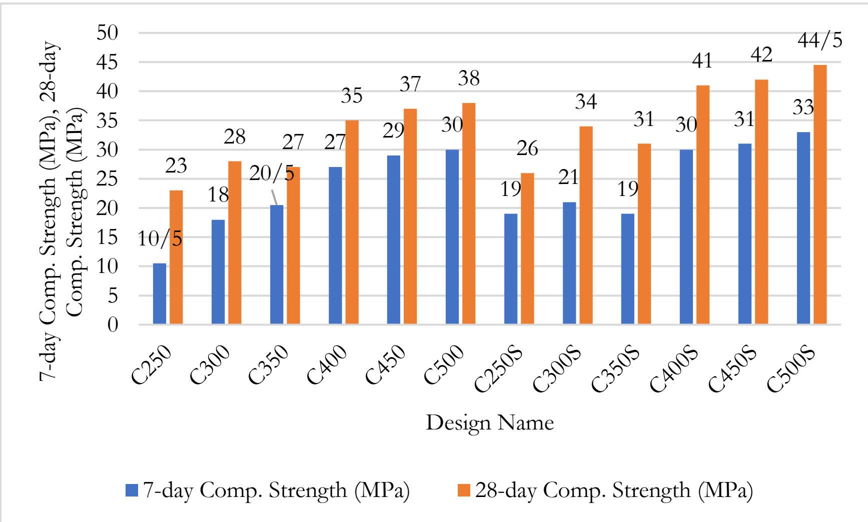

Fig. 7. Compressive strength of 7 and 28 days for all designs.

3.4 | The Relationship between the Amount of Powder Materials and the Slum of the Samples

The study investigates how the amount of powder materials (a combination of cement and micro-silica) influences concrete mixes' slump or workability. This relationship is essential in construction as slump values indicate how easy it is to handle, place, and compact the concrete, impacting construction processes' overall quality and efficiency [47]. Workability, assessed through the slump test, is particularly important when the concrete must flow easily, such as in structures with complex reinforcement layouts or narrow formwork [48]. The results, illustrated in *Fig. 8*, show a positive correlation between the powder material content and slump values. As the grade of cement and total powder content in the mix increases, the slump values rise correspondingly. This trend can be mathematically expressed through two separate equations: one for mixes without micro-silica and one for mixes with micro-silica. For concrete without micro-silica, the relationship follows the equation $Y = 0.016X + 2.333$, with a high correlation coefficient ($R^2 = 0.9465$). Similarly, for concrete mixes containing micro-silica, the relationship is represented by $Y = 0.0169X + 1.2619$, with an R^2 of 0.9412. In both cases, X represents the powder content (kg/m^3) and Y denotes the slump (cm). The high R^2 values indicate a strong linear relationship, signifying that increases in powder material content reliably predict increases in a slump. The primary reason for this increase in slump with higher powder content is the enhanced paste volume in the mix. A more significant amount of cement and micro-silica contributes to a greater cement paste volume, making the concrete mixture more cohesive and fluid. This increased paste volume provides better lubrication within the mix, allowing it to flow more readily, reflected in the higher slump values. As a result, concrete with higher powder content is more workable, making it easier to handle, place, and compact during construction, especially for projects that require high fluidity in the concrete. Interestingly, the study also found that adding micro-silica slightly reduces the slump compared to similar mixes without micro-silica. This reduction is attributed to the unique properties of micro-silica particles, which are much finer than cement particles and have a higher specific surface area. This increased surface area leads to a greater demand for water to fully hydrate the particles, which means more water is absorbed by the micro-silica, leaving less free water available for concrete flow. As a result, the mixture becomes less fluid, reflected in the slightly lower slump values. Despite the minor reduction in workability, micro-silica offers significant strength and durability benefits, making it a valuable addition to high-performance concrete, particularly in applications requiring enhanced long-term strength and durability. The study underscores a clear relationship between powder material content and workability in concrete mixes. While higher cement and micro-silica content enhance the slump and thus the workability, including micro-silica requires careful consideration due to its water absorption properties. Optimizing the proportions of cement and micro-silica for construction applications that demand a balance between workability and strength is crucial [48]. By carefully adjusting these components, engineers can achieve a concrete mix that meets specific workability requirements without compromising strength or durability. This insight is precious for projects where fluidity and ease of placement are essential, alongside the need for robust long-term performance.

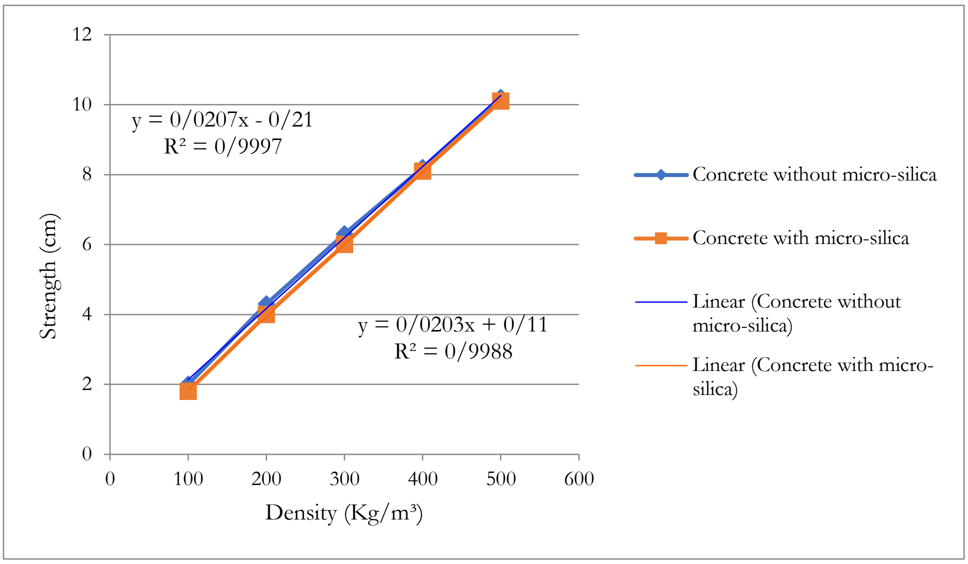

Fig. 8. The relationship between the amount of powdered materials and the slum of the samples.

3.5 | The Relationship between the Amount of Powder Materials and the Compressive Strength of the Samples

3.5.1 | Effect of micro-silica on early strength

Figs. 9 and *10* demonstrate the relationship between the number of cementitious materials, including cement and micro-silica, and the compressive strength of concrete at 7 and 28 days, respectively. These figures reveal a clear trend: As the grade of cement and total cementitious material content increase, the compressive strength of the concrete samples also rises, both at early (7-day) and long-term (28-day) ages. In *Fig. 9*, which focuses on /-day compressive strength, linear equations for both concrete with and without micro-silica were derived, with excellent correlation values (R^2 values close to 1). The equation for micro-silica-free concrete is given as $Y = 0.066X + 0.2$ with an R^2 of 0.9991, while for concrete with micro-silica, the equation is $Y = 0.063X - 1.5$ with an R^2 of 0.9992. Here, X represents the number of cementitious materials in kg/m^3, and Y is the compressive strength in MPa. The high R^2 values indicate strong linear relationships, confirming that increased powder content significantly enhances the early-age strength of the concrete. In *Fig. 10*, illustrating 28-day compressive strength, similar linear relationships were established. For concrete without micro-silica, the equation $Y = 0.063X + 9.1 (R^2 = 0.9972)$ was derived, while for concrete with micro-silica, the equation $Y = 0.068X + 11.6 (R^2 = 0.9966)$ was determined. Again, X represents the number of cementitious materials, and Y denotes the 28-day compressive strength. The slightly higher slope for micro-silica-containing concrete indicates that micro-silica addition has a positive impact on long-term strength. The observed increase in compressive strength at both 7 and 28 days can be attributed to the higher cement content, which provides more binding material, enhancing the strength development process. Furthermore, the addition of 10% micro-silica contributes significantly to this strength increase, especially at later stages. Initially, at very young ages (such as 1 to 3 days), micro-silica may slightly reduce strength due to decreased heat of hydration. However, as the concrete cures, microsilica contributes to filling micro-pores and enhances particle packing through pozzolanic reactions, which lead to a denser and stronger microstructure.

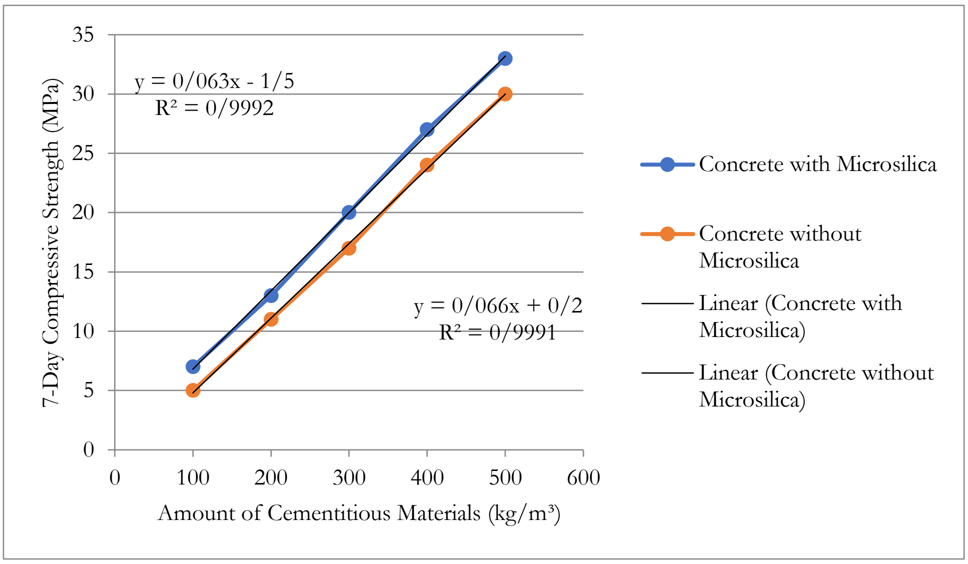

Fig. 9. The relationship between the amount of powder materials and the compressive strength of 7 days.

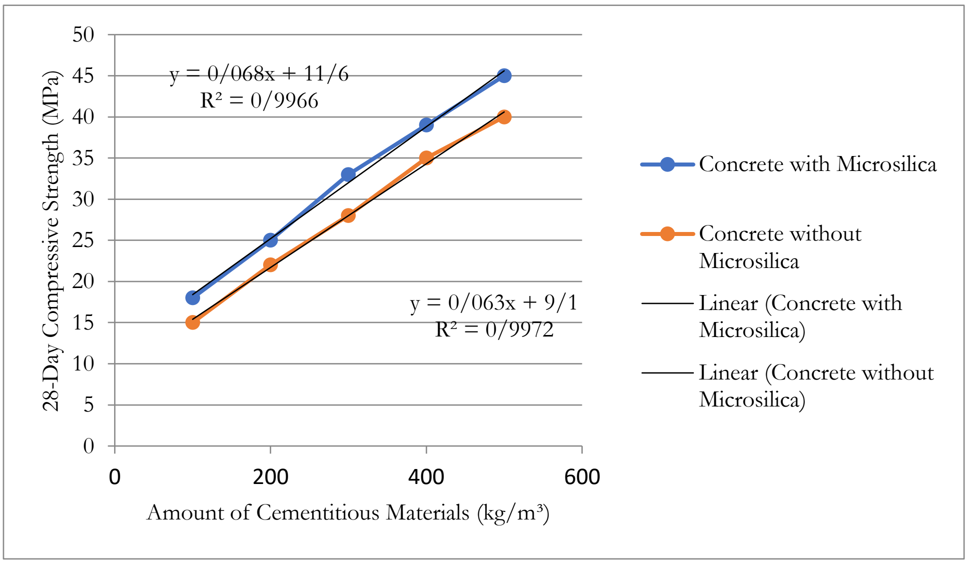

Fig. 10. The relationship between the amount of powder materials and the compressive strength of 28 days.

3.6 | The Relationship between 7-Day and 28-Day Compressive Strength of the Samples

Fig. 11 illustrates the relationship between the 7-day and 28-day compressive strengths for concrete samples with and without micro-silica. This relationship is essential for predicting the long-term compressive strength of concrete based on its early-age strength. The data in this figure, which are fitted with high accuracy (R^2 values of 0.9897 for concrete with micro-silica and 0.9947 for concrete without micro-silica), reveal strong linear correlations between the compressive strengths at these two curing ages. For micro-silica-free concrete, the linear relationship is represented by the equation: $Y = 1.0357X + 11.143$ where Y is the 28-day compressive strength (in MPa) and X is the 7-day compressive strength (in MPa). The high R^2 value (0.9947) indicates that this equation accurately predicts the 28-day strength based on the 7-day strength in concrete without micro-silica. For concrete containing micro-silica, the relationship follows a slightly different equation: $Y = 1.0857X + 12.714$. This equation also has a strong correlation ($R^2 = 0.9897$), suggesting that 28-day strength can be reliably predicted from 7-day strength for concrete with micro-silica. These equations demonstrate that as the 7-day compressive strength increases, the 28-day compressive strength also increases, with concrete containing micro-silica showing a marginally steeper slope. This steeper slope indicates that micro-silica enhances the long-term gain relative to 7-day strength, likely due to its pozzolanic reactions, which continue to densify the concrete matrix over time. Additionally, using SPSS software, a more generalized Eq was derived to predict 28-day Compressive Strength (CS28) based on multiple factors, including 7-day Compressive Strength (CS7), cement grade (C), and micro-Silica Content (SF). The regression equation obtained is

$$\mathrm{CS28} = 13.852 + 0.011\mathrm{C} + 0.073\mathrm{SF} + 0.689\mathrm{CS7},$$

where

I. CS28: 28-day compressive strength in MPa.

II. C: Cement grade in $\mathrm{kg/m^3}$.

III. SF: Micro-silica content in $\mathrm{kg/m^3}$.

IV. CS7: 7-day compressive strength in MPa.

This regression model, with an R^2 value of 0.958 indicates that these parameters (cement grade, micro-silica amount, and early-age strength) together provide a reliable prediction for the 28-day compressive strength, highlighting the influence of each component in long-term strength development.

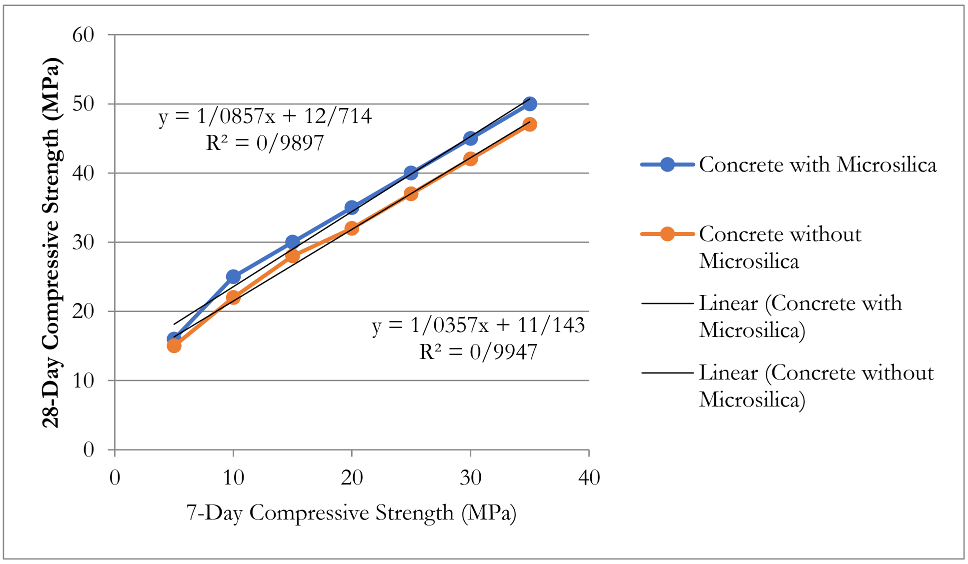

Fig. 11. The relationship between 7-day and 28-day compressive strength of the samples.

Fig. 12.a shows how variations in cement grade (C) influence CS28. The blue dots represent actual CS28 values, while the green dashed line shows predicted CS28 based on the model. As the cement grade increases, there is a corresponding increase in CS28, suggesting that higher cement grades contribute to higher long-term strength. *Fig. 12.b* illustrates the relationship between the amount of micro-silica (SF) and CS28. The orange markers are the actual CS28 values, and the green dashed line represents the model's predictions. The graph shows that as micro-silica content increases, the 28-day compressive strength also rises, although this effect may plateau at higher levels. Micro-silica positively contributes to concrete strength by enhancing the concrete matrix's density. *Fig. 12.c* presents the correlation between 7-day compressive strength (CS7) and CS28. The purple markers denote actual CS28 values, and the green dashed line indicates predicted values.

This plot highlights a robust positive relationship, suggesting that early-age strength (CS7) is a good predictor of long-term compressive strength (CS28).

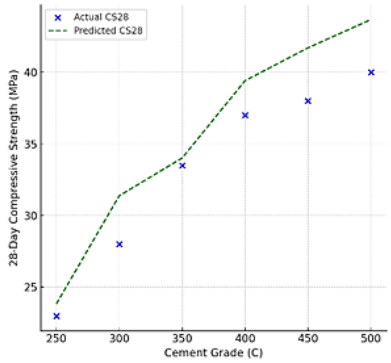

a.

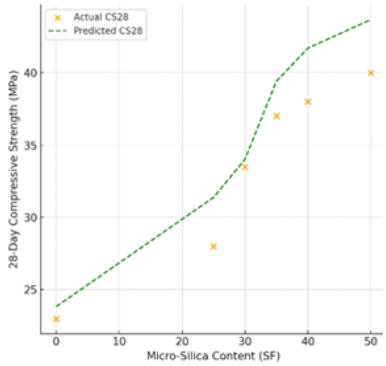

b.

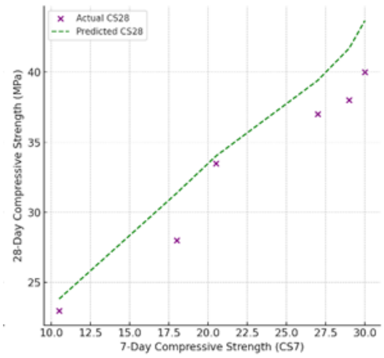

c.

Fig. 12. Results of statistical analysis using spss 22 software to predict; a. The effect of cement grade on 28-day strength, b. The effect of micro-silica on 28-day strength, and c. The effect of 7-day strength on 28-day strength.

3.7 | Prediction of 28-Day Compressive Strength of Concretes Using Neural Networks

The neural network model developed using MATLAB's neural net fitting toolkit aimed to predict the 28-day compressive strength of concrete based on input factors like 7-day compressive strength, cement grade, and micro-silica content. The model employed a two-layer architecture with hyperbolic tangent activation functions and included seven neurons in the first layer to optimize prediction accuracy. To ensure robust training, 70% of the data was allocated for training, 15% for validation, and 15% for testing. *Fig. 13* compares the predicted 28-day compressive strength against actual laboratory measurements, with the expected points closely aligning along a 1:1 line, showcasing the model's accuracy. The high correlation coefficient of $R = 0.99$ and the derived regression equation Output $= 0.94 \times$ Target $+1.9$ emphasize the precision of the neural network. This close agreement between predicted and actual values highlights the neural network's effectiveness in forecasting long-term concrete strength, demonstrating its potential as a reliable tool for optimizing early construction planning. Material quality control is based on initial concrete properties.

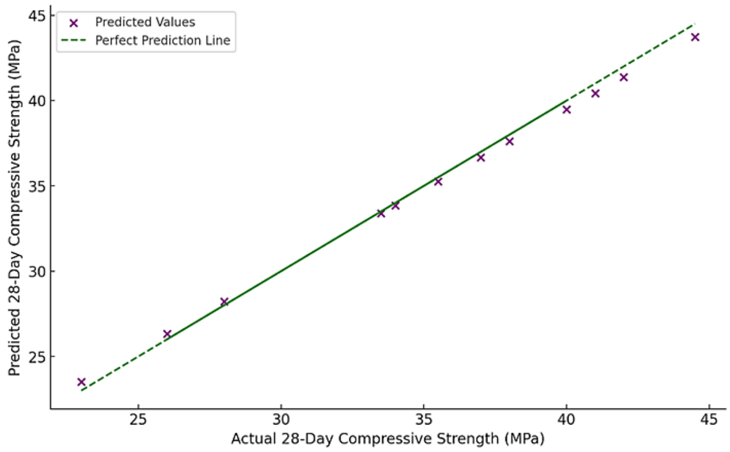

Fig. 13. Neural network model prediction of 28-day compressive strength of concrete.

The model's performance and accuracy are shown in *Fig. 13*, where individual regression plots for training, validation, and testing data are provided, along with a combined plot for the entire dataset. The predicted 28-day compressive strengths (the ANN's outputs) are plotted against the actual 28-day strengths (the target values from laboratory tests) in each of these plots. Ideally, the points in these plots align closely along the diagonal line, indicating accurate predictions. The high degree of alignment suggests that the model effectively captured the relationship between inputs and the target output. The regression coefficient (R) for this plot is 0.99, an exceptionally high value that indicates a near-perfect correlation between the predicted and actual values. This high R-value demonstrates that the model has successfully captured the underlying patterns in the data, leading to highly accurate predictions. An additional equation derived from the network's output and target values further illustrates the model's accuracy.

$$\text{Output} = 0.94 \times \text{Target} + 1.9. \quad (8)$$

In this equation, the "output" represents the predicted 28-day compressive strength, while the "Target" refers to the actual compressive strength obtained from laboratory results. The close alignment between these values, as indicated by the regression coefficient of 0.99, confirms the effectiveness of the neural network model.

Fig. 14 illustrates the neural network's performance in predicting 28-day compressive strength across four stages: a) Training, b) Validation, c) Testing, and d) Overall Performance. In the training phase (*Fig. 14.a*), the network successfully fit with actual data, as indicated by the regression line output $\approx 0.95 \times$ target $+1.6$ and a high correlation value (R = 0.99429). During validation (*Fig. 14.b*), the model demonstrated perfect prediction alignment, with an R value of 1, indicating its ability to generalize well to new data. Similarly, in the testing phase (*Fig. 14.c*), the network maintained excellent predictive accuracy, achieving an R value of 1, with a regression line output ≈ 0.8 × target + 6.3. When combining all data (*Fig. 14.d*), the network showed consistent accuracy across all stages, yielding an overall R value of 0.99213, with the regression line output ≈ 0.94 × Target +1.9. These results confirm the network's robustness and reliability in predicting compressive strength with high precision across different data subsets, making it a valuable tool for concrete strength estimation.

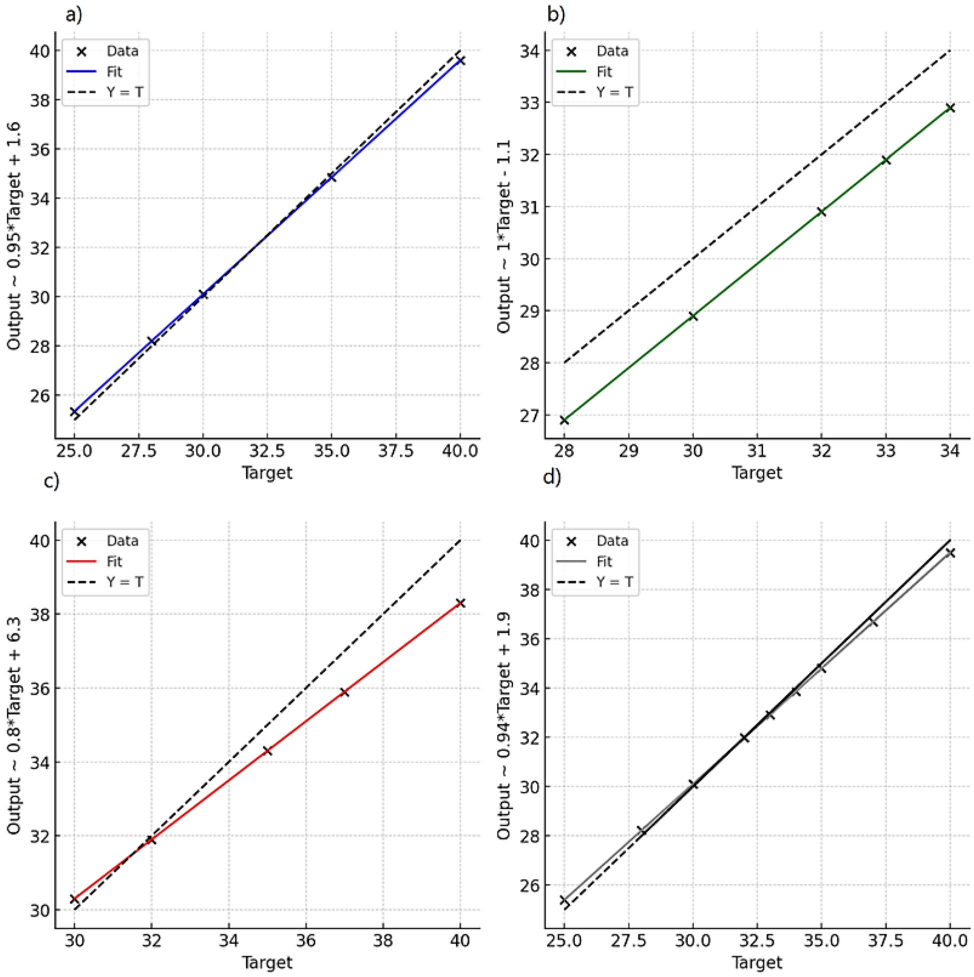

Fig. 14. The neural network's performance in predicting 28-day compressive strength; a. Training (R=0.994), b. Validation (R=1.0), c. Testing (R=1.0), and d. Overall (R=0.992).

This study comprehensively evaluated the effects of varying cement content and the addition of micro-silica on the workability and compressive strength of twelve distinct concrete mix designs. The primary objectives were to assess the influence of these variables on concrete's slump (workability) and compressive strength at early (7-day) and long-term (28-day) ages. Slump tests showed that increased cement content led to higher workability, as indicated by greater slump values, due to the increased paste volume, which enhances fluidity. Micro-silica addition, while slightly reducing slump due to its water-absorbing properties, contributed positively to the strength of the mixes, showing a minor trade-off between workability and strength. S.T.1 illustrates the primary components that make up cement, such as limestone, clay, and gypsum. The balance achieved here was crucial, as it allowed for optimized mixes that enhanced strength while retaining reasonable workability. The compressive strength tests provided valuable insights into the early and long-term performance of the concrete mixes. Consistent with the objectives, the study found that both higher cement content and the inclusion of micro-silica contributed significantly to strength gains. Mixes with higher cement grades exhibited superior compressive strength at both 7 and 28 days, confirming the role of cement as a critical factor in strength development. The addition of micro-silica, particularly at a 10% replacement level, further enhanced long-term strength through pozzolanic reactions, contributing to a denser microstructure. This resulted in concrete mixes that not only gained strength more rapidly but also achieved higher ultimate strength at 28 days. These findings underscore the role of micro-silica in improving both early and long-term performance, especially for structural applications requiring enhanced durability and strength. Statistical and neural network models were applied to forecast 28-day compressive strength based on variables such as 7-day compressive strength, cement grade, and micro-silica content to advance predictive capabilities. S.T.2 highlights the main chemical compounds found in cement, including tricalcium silicate (C_3S) and dicalcium silicate (C_2S), and their properties like setting time and strength contribution. The regression model generated using SPSS yielded a high R^2 value, indicating a reliable prediction of 28-day strength from these inputs. The neural network model demonstrated remarkable accuracy, with an overall correlation coefficient of 0.99, reflecting its robustness in capturing complex relationships between the input factors and compressive strength outcomes. S.T.3 provides an overview of the different types of PC and their specific characteristics, such as Type I for general use and Type III for high early strength. This model's successful predictions demonstrate its potential for practical applications, allowing for early concrete strength estimation, which can inform timely decision-making in construction projects. In the 3D-Printed Concrete (3DPC) study, various aggregate types have been explored for their impact on compressive strength and other mechanical properties. For example, Recycled Fine Aggregate (RFA) offers unique advantages under extreme conditions. According to [49], the high porosity of RFA helps mitigate the risk of blast spalling during high-temperature explosions, making it beneficial in certain applications. S.T.4 shows the allowable maximum concentration of harmful substances in water used for concrete mixing, ensuring safe and durable concrete production. However, including RFA typically results in a slight reduction in compressive strength compared to non-RFA-doped 3DPC, as shown in [50]. Recycled Coarse Aggregate (RCA) exhibits a more pronounced effect on compressive strength, with studies indicating a progressive decrease in strength as the RCA replacement ratio increases [51]. This trend suggests that RCA may be less suitable for applications requiring high load-bearing capacity in 3DPC. When RFA and RCA are combined, [51] reports a reduction in the hardening properties of the printed concrete. However, this combination appears to reduce anisotropy in compressive strength across different orientations, which could be advantageous in achieving uniform performance in printed structures. S.T.5 categorizes various concrete additives, detailing their functions such as water reducers, accelerators, and air-entraining agents. Crumb rubber has been shown to improve the compressive strength of 3DPC, although it introduces significant anisotropy, as noted in [52]. This anisotropic behavior indicates variability in strength based on the printing direction, a factor that must be carefully considered in structural design. Coral sand, conversely, reduces the compressive strength of 3DPC, as reported in [43]. This limitation suggests that coral sand may be less suitable for structural applications where compressive strength is a critical parameter. Calcium carbonate as an aggregate in 3DPC has demonstrated favorable compressive strength, per findings in [53]. This indicates its potential as a viable aggregate for enhancing the structural performance of 3DPC. In conclusion, although the use of certain aggregates, such as RFA and RCA, may reduce compressive strength, benefits such as enhanced spalling resistance and reduced anisotropy are provided. Aggregates like crumb rubber and calcium carbonate show promise in enhancing compressive strength, though with considerations of anisotropy in the case of crumb rubber. This analysis highlights the need for a tailored approach in aggregate selection based on the specific performance requirements of 3DPC applications. Incorporating various fiber types into 3DPC significantly affects its compressive strength and mechanical anisotropy. Steel fibers, for instance, have been shown to create anisotropic properties within 3DPC due to their directional distribution during the printing process [54]. The anisotropy level is closely linked to the fiber content, with higher fiber concentrations amplifying this effect [55], [56]. Furthermore, the unique nature of the 3D printing process can influence fiber distribution, potentially enhancing compressive strength in specific orientations as the fibers align more effectively [57]. In contrast, basalt fibers, despite their alignment along the printing direction, tend to reduce compressive strength at contents of 0.85% and 1% [53], [58]. However, basalt fibers exhibit superior load-bearing capacity when aligned with the X-axis, demonstrating their directional strength [59]. Other fiber types, such as glass and carbon fibers, exhibit different impacts on 3DPC properties. Glass fibers do not notably affect the anisotropy of 3DPC. However, a reduction in compressive strength has been associated with their use [53], [60], [61]. Carbon fibers, particularly at a 0.5% content, result in a modest compressive strength increase of less than 10% [62]. However, an oxidation treatment on carbon fibers' surfaces further enhances compressive strength, likely due to improved bonding within the concrete matrix [63]. Poly Vinyl Alcohol (PVA) fibers reinforce 3DPC with marked mechanical anisotropy, especially in the Y and Z axes, where higher fiber contents significantly increase compressive strength [64], [65]. Similarly, polypropylene fibers contribute to improved compressive strength and anisotropic mechanical properties due to their effective filling effect within the matrix [66], [67]. Overall, the choice of fiber type and its alignment relative to the printing direction are key factors that must be carefully managed to optimize compressive strength and control anisotropy in 3DPC applications. Overall, this study achieved its objectives, contributing valuable insights into the relationship between mix composition and concrete properties. The study offers practical guidance for producing high-performance concrete by optimizing cement and micro-silica content. The predictive models developed here provide a reliable means of estimating concrete strength based on early-age properties, supporting efficient planning and quality control in construction. These findings contribute to the growing body of knowledge on high-performance concrete mixes and underscore the importance of innovative modeling approaches in enhancing predictive accuracy, which can be foundational for future research and applications in structural engineering. S.T.6 lists the typical concrete mix components and their approximate proportions, including aggregates, cement, water, and any added admixtures. S.T.7 depicts the chemical characteristics of cement used, discussing factors like alkali content, sulfate resistance, and heat of hydration. S.F.1 compares the minimum and maximum typical percentages of various components in cement. Lime (CaO) has the highest concentration range, followed by silica (SiO_2), while other components such as alumina (Al_2O_3), iron oxide (Fe_2O_3), and alkalis (Na_2O) have significantly lower percentages. This distribution indicates the dominance of lime and silica in cement composition. S.F.2 shows the maximum allowable concentrations of harmful substances in concrete water, measured in parts per million (ppm). Dissolved solids have the highest permissible concentration at 35,000 ppm, followed by chlorides at 10,000 ppm and sulfates (SO_4^{2-}) at 3,000 ppm. Solid particulate matter and alkalis have much lower concentration limits, indicating a need for tighter control over these substances. S.F.3 displays the constituent percentages of chemical compositions in cement. CaO dominates the composition at over 60%, followed by silicon dioxide (SiO_2) at around 20%. Other compounds like alumina (Al_2O_3), iron oxide (Fe_2O_3), magnesium oxide (MgO), and trace elements such as potassium oxide (K_2O), sodium oxide (Na_2O), sulfur trioxide (SO_3), and LOI are present in smaller amounts, highlighting CaO as the primary component in cement.

4 | Conclusion

This study demonstrates that optimizing cement content and including micro-silica in concrete mixes significantly enhance workability and compressive strength, offering practical insights for high-performance concrete applications. Precisely, mixes with 500 kg/m³ cement content, such as C500 and C500S, achieved slump values of 10 cm, reflecting excellent workability. This increased workability is attributed to a higher paste volume, facilitating ease of placement and finishing. Despite slightly reducing workability due to its water absorption properties, the addition of micro-silica provided substantial strength gains. For instance, at 7 days, C500S reached a compressive strength of 33 MPa compared to 30 MPa in C500, while at 28 days, C500S achieved a peak strength of 44.5 MPa, highlighting micro-silica's role in densifying the concrete matrix through pozzolanic reactions. The predictive models developed in this study further validate these findings, offering high accuracy in estimating 28-day strength. The statistical regression model yielded an R^2 of 0.958, indicating reliable predictions of 28-day strength based on early-age properties. Similarly, the neural network model achieved an overall correlation coefficient (R) of 0.99, accurately capturing complex relationships among 7-day strength, cement grade, and micro-silica content. The regression equation derived from the neural network model, output ≈ 0.94 × target + 1.9, underscores its precision, providing a valuable tool for early strength estimation that supports efficient project planning and quality control. Comparing these results with recent findings in 3DPC, the study shows that specific aggregate and fiber types influence concrete's mechanical properties. For instance, RFA enhances high-temperature resistance but slightly lowers compressive strength. In contrast, RCA leads to a more noticeable strength reduction as replacement ratios increase. Similarly, fibers like steel and polypropylene enhance compressive strength and mechanical anisotropy in 3DPC, whereas basalt and glass fibers tend to reduce strength when used at certain levels. This research successfully achieves its goals by providing concrete mix designs that balance workability and compressive strength for structural applications. The predictive models contribute significantly to construction management by enabling early adjustments in mix design to meet specified strength requirements. This study offers a robust foundation for future work in optimizing concrete properties and enhancing predictive accuracy, advancing the capabilities of high-performance concrete in modern construction.

References

[1] Kumar, R., Kumar, S., Rai, B., & Samui, P. (2024). Development of hybrid gradient boosting models for predicting the compressive strength of high-volume fly ash self-compacting concrete with silica fume. *Structures*, *66*, 106850. https://doi.org/10.1016/j.istruc.2024.106850

[2] Okamura, H., & Ouchi, M. (2003). Self-compacting concrete. *Journal of advanced concrete technology*, *1*(1), 5–15. https://doi.org/10.3151/jact.1.5

[3] Ozawa, K., Maekawa, K., Kunishima, M., & Okamura, H. (1989). High performance concrete based on the durability design of concrete structures. *Proceedings of the second East Asia-Pacific conference on structural engineering and construction* (pp. 445–450). Asian Institute of Technology.

[4] Khayat, K. H. (1999). Workability, testing, and performance of self-consolidating concrete. *Materials journal*, *96*(3), 346–353. https://www.researchgate.net/profile/Kamal-Khayat/publication/279902414

[5] Kumar, S., & Rai, B. (2019). Pulse velocity–strength and elasticity relationship of high volume fly ash induced self-compacting concrete. *Journal of structural integrity and maintenance*, *4*(4), 216–229. https://doi.org/10.1080/24705314.2019.1657615

[6] Kumar, S., & Rai, B. (2022). Synergetic effect of fly ash and silica fume on the performance of high volume fly ash self-compacting concrete. *Journal of structural integrity and maintenance*, *7*(1), 61–74. https://doi.org/10.1080/24705314.2021.1892571

[7] Kumar, S., Rai, B., Biswas, R., Samui, P., & Kim, D. (2020). Prediction of rapid chloride permeability of self-compacting concrete using multivariate adaptive regression spline and minimax probability machine regression. *Journal of building engineering*, *32*, 101490. https://doi.org/10.1016/j.jobe.2020.101490

[8] Kumar, S., Kumar, D. R., Wipulanusat, W., & Keawsawasvong, S. (2024). Development of ANN-based metaheuristic models for the study of the durability characteristics of high-volume fly ash self-compacting concrete with silica fume. *Journal of building engineering*, *94*, 109844. https://doi.org/10.1016/j.jobe.2024.109844

[9] Wang, J., Du, P., Zhou, Z., Xu, D., Xie, N., & Cheng, X. (2019). Effect of nano-silica on hydration, microstructure of alkali-activated slag. *Construction and building materials*, *220*, 110–118. https://doi.org/10.1016/j.conbuildmat.2019.05.158

[10] Assaedi, H., Shaikh, F. U. A., & Low, I. M. (2016). Influence of mixing methods of nano silica on the microstructural and mechanical properties of flax fabric reinforced geopolymer composites. *Construction and building materials*, *123*, 541–552. https://doi.org/10.1016/j.conbuildmat.2016.07.049

[11] A Louis, M. (2010). Strength of reactive silica sand powder concretemade of local powders. *Al-qadisiyah journal for engineering sciences*, *3*(3), 234–243. https://qjes.qu.edu.iq/article_12872.html

[12] Abd El-Baky, S., Yehia, S., & Khalil, I. S. (2013). Influence of nano-silica addition on properties of fresh and hardened cement mortar. *Nanocon brno* (pp. 16–18). Tanger, s.r.o. https://www.researchgate.net/publication/309592647

[13] Chaudhary, J. L., Harison, A., & Srivastava, V. (2015). Use of silica sand as cement replacement in ppc concrete. *International journal of research in engineering and technology*, *4*(11), 55–58. https://www.researchgate.net/publication/291075241

[14] Chalmers, D., MacKenzie, N. G., & Carter, S. (2021). Artificial intelligence and entrepreneurship: Implications for venture creation in the fourth industrial revolution. *Entrepreneurship theory and practice*, *45*(5), 1028–1053. https://doi.org/10.1177/1042258720934581

[15] Lee, J., Davari, H., Singh, J., & Pandhare, V. (2018). Industrial artificial intelligence for Industry 4.0-based manufacturing systems. *Manufacturing letters*, *18*, 20–23. https://doi.org/10.1016/j.mfglet.2018.09.002

[16] Arslan Hafeez, M., Usman, M., Umer, M. A., & Hanif, A. (2020). Recent progress in isotropic magnetorheological elastomers and their properties: A review. *Polymers*, *12*(12), 1–34. https://doi.org/10.3390/polym12123023

[17] Shah, M. U., Usman, M., Farooq, S. H., & Rizwan, M. (2023). Spring-controlled modified tuned liquid column ball damper for vibration mitigation of structures. *Journal of sound and vibration*, *545*, 117443. https://doi.org/10.1016/j.jsv.2022.117443

[18] Lwakatare, L. E., Raj, A., Crnkovic, I., Bosch, J., & Olsson, H. H. (2020). Large-scale machine learning systems in real-world industrial settings: A review of challenges and solutions. *Information and software technology*, *127*, 106368. https://doi.org/10.1016/j.infsof.2020.106368

[19] Laskar, A., & Murty, C. V. R. (2004). *Challenges before construction industry in India*. https://www.iitk.ac.in/nicee/RP/2004_Challenges_Construction_Industry_Proceedings.pdf

[20] Ofori, G. (2000). Challenges of construction industries in developing countries: Lessons from various countries. *2nd international conference on construction in developing countries: Challenges facing the construction industry in developing countries* (pp. 1–11). International Council for Research and Innovation in Building and Construction (CIB). https://www.researchgate.net/publication/242410723

[21] Waqas, H. A., Sahil, M., Khan, M. M., Anwar, A. W., Shah, M. U., & Usman, M. (2024). Optimizing reinforcement strategies for robust beam-column joints in seismic-resistant structures. *Arabian journal for science and engineering*, *49*(4), 6107–6124. https://doi.org/10.1007/s13369-023-08591-1

[22] Abbasi, S., Umer, M. A., Irfan, M., Siyar, M., Usman, M., & Masood, M. T. (2023). Enhanced mechanical properties of surface modified and silica reinforced nomex sandwich composites. *Materials today communications*, *36*, 106346. https://doi.org/10.1016/j.mtcomm.2023.106346

[23] Ji, Y., Li, K., Liu, G., Shrestha, A., & Jing, J. (2018). Comparing greenhouse gas emissions of precast in-situ and conventional construction methods. *Journal of cleaner production*, *173*, 124–134. https://doi.org/10.1016/j.jclepro.2016.07.143

[24] Malik, U. J., Riaz, R. D., Rehman, S. U., Usman, M., Riaz, R. E., & Hamza, R. (2024). Advancing mix design prediction in 3D printed concrete: Predicting anisotropic compressive strength and slump flow. *Case studies in construction materials*, *21*, e03510. https://doi.org/10.1016/j.cscm.2024.e03510

[25] Rehman, S. U., Usman, M., Toor, M. H. Y., & Hussaini, Q. A. (2024). Advancing structural health monitoring: A vibration-based IoT approach for remote real-time systems. *Sensors and actuators a: Physical*, *365*, 114863. https://doi.org/10.1016/j.sna.2023.114863

[26] Fikri Hasmori, M., Faizul Md Zin, A., Nagapan, S., Deraman, R., Abas, N., Yunus, R., & Klufallah, M. (2020). The on-site waste minimization practices for construction waste. *IOP conference series: Materials science and engineering*, *713*(1), 12038. https://doi.org/10.1088/1757-899X/713/1/012038

[27] Adesina, A. D. (2018). Concrete sustainability issues. *Proceedings of the 38th cement and concrete science conference* (pp. 24–26). Coventry University. https://spectrum.library.concordia.ca/id/eprint/984818/

[28] Jaillon, L., & Poon, C. (2010). Design issues of using prefabrication in Hong Kong building construction. *Construction management and economics*, *28*(10), 1025–1042. https://doi.org/10.1080/01446193.2010.498481

[29] Azhar, S., Lukkad, M. Y., & Ahmad, I. (2013). An investigation of critical factors and constraints for selecting modular construction over conventional stick-built technique. *International journal of construction education and research*, *9*(3), 203–225. https://doi.org/10.1080/15578771.2012.723115

[30] Arumsari, P., & Xavier, C. (2020). Cost and time analysis on the selection of formwork installation method. *IOP conference series: Earth and environmental science*, *426*(1), 12042. https://doi.org/10.1088/1755-1315/426/1/012042

[31] Kangari, R., & Yoshida, T. (1990). Automation in construction. *Robotics and autonomous systems*, *6*(4), 327–335. https://doi.org/10.1016/S0921-8890(05)80014-4

[32] Dilawar Riaz, R., Usman, M., Ali, A., Majid, U., Faizan, M., & Jalil Malik, U. (2023). Inclusive characterization of 3D printed concrete (3DPC) in additive manufacturing: A detailed review. *Construction and building materials*, *394*, 132229. https://doi.org/10.1016/j.conbuildmat.2023.132229

[33] Zou, D., Xiao, L., Zhang, Y., & Li, H. (2023). Effect of hexadecyltrimethoxysilane modified micro silica particles on workability and compressive strength of ultra-high-performance concrete. *Construction and building materials*, *399*, 132480. https://doi.org/10.1016/j.conbuildmat.2023.132480

[34] Casagrande, C. A., Jochem, L. F., Onghero, L., Ricardo de Matos, P., Repette, W. L., & Gleize, P. J. P. (2020). Effect of partial substitution of superplasticizer by silanes in Portland cement pastes. *Journal of building engineering*, *29*, 101226. https://doi.org/10.1016/j.jobe.2020.101226

[35] Chen, B., Shao, H., Li, B., & Li, Z. (2020). Influence of silane on hydration characteristics and mechanical properties of cement paste. *Cement and concrete composites*, *113*, 103743. https://doi.org/10.1016/j.cemconcomp.2020.103743

[36] Hamada, H. M., Abed, F., & Hassan, A. (2024). Combined effect of iron ore waste and basalt fiber with high-volume supplementary cementitious materials on the workability, strength, and microstructure of sustainable concrete. *Construction and building materials*, *444*, 137679. https://doi.org/10.1016/j.conbuildmat.2024.137679

[37] Peng, G., Wu, J., Huang, K., Shi, C., Hu, X., & Niu, D. (2024). Research on workability, mechanics, and durability of cementitious grout: A critical review. *Construction and building materials*, *449*, 138374. https://doi.org/10.1016/j.conbuildmat.2024.138374

[38] Alebra, A. (2023). *Behavior analysis of cement concrete with combination of waste rubber and glass*. https://digitalcommons.kennesaw.edu/undergradsymposiumksu/spring2023/presentations/86/

[39] Jiang, J., Wang, W., Shen, H., Wang, J., & Cao, J. (2017). Characterization of silica particles modified with γ-methacryloxypropyltrimethoxysilane. *Applied surface science*, *397*, 104–111. https://doi.org/10.1016/j.apsusc.2016.11.075

[40] Amini, M. M., Ghanepour, M., & Rezaifar, O. (2024). Experimental analysis of the impact of alternating magnetic fields on the compressive strength of concrete with various silica sand and microsilica compositions. *Case studies in construction materials*, *21*, e03487. https://doi.org/10.1016/j.cscm.2024.e03487

[41] Wang, Y., Xu, L., Li, J., Li, Y., Zhou, Y., Liu, W., … ., & Zhang, Y. (2024). Development and optimization of an artificial neural network (ANN) model for predicting the cadmium fixation efficiency of biochar in soil. *Journal of environmental chemical engineering*, *12*(6), 114196. https://doi.org/10.1016/j.jece.2024.114196

[42] Uraz, E., Hayri-Senel, T., Erdol-Aydin, N., & Nasun-Saygili, G. (2024). Removal of zinc from wastewaters using Turkish bentonite and artificial neural network [ANN] modeling. *Heliyon*, *10*(20), e39080. https://doi.org/10.1016/j.heliyon.2024.e39080

[43] Majumder, R., & Mishra, S. K. (2024). Reliability consistent knockdown factors for truncated conical shells via artificial neural network (ANN) based predictions and meta-modelling. *Thin-walled structures*, *205*, 112541. https://doi.org/10.1016/j.tws.2024.112541

[44] Liu, M., Wang, H., Shi, H., Zhang, B., Sun, X., & Wang, J. (2024). Examining the personal growth of college teacher educators through the lens of human development ecology: An approach utilizing artificial neural networks (ANNs) modeling. *Heliyon*, *10*(21), e39372. https://doi.org/10.1016/j.heliyon.2024.e39372

[45] Mohamed, O. A., Najm, O., Zuaiter, H. A., Saleem, S. K., Ivak, S., & Al-Aribe, K. (2024). Effect of activator concentration on setting time, workability and compressive strength of sustainable concrete with alkali-activated slag binder. *Materials today: Proceedings*. Elsevier. https://doi.org/10.1016/j.matpr.2024.04.103

[46] Al Rifai, M. M., Sikora, K. S., & Hadi, M. N. S. (2024). Effect of micro steel fibers volume fraction on behavior of high-strength self-compacting concrete. *Construction and building materials*, *450*, 138709. https://doi.org/10.1016/j.conbuildmat.2024.138709

[47] Zhu, C., Zhang, S., Liu, C., Dang, Q., & Bai, G. (2024). Study on the properties of recycled concrete mixed with coal gangue: Mechanics, workability and microstructure. *Journal of building engineering*, *98*, 111065. https://doi.org/10.1016/j.jobe.2024.111065

[48] Ma, H., Zhu, H., Wu, C., Chen, H., Sun, J., & Liu, J. (2020). Study on compressive strength and durability of alkali-activated coal gangue-slag concrete and its mechanism. *Powder technology*, *368*, 112–124. https://doi.org/10.1016/j.powtec.2020.04.054

[49] Xiao, J., Han, N., Zhang, L., & Zou, S. (2021). Mechanical and microstructural evolution of 3D printed concrete with polyethylene fiber and recycled sand at elevated temperatures. *Construction and building materials*, *293*, 123524. https://doi.org/10.1016/j.conbuildmat.2021.123524

[50] Bai, M., Wu, Y., Xiao, J., Ding, T., & Yu, K. (2023). Workability and hardened properties of 3D printed engineered cementitious composites incorporating recycled sand and PE fibers. *Journal of building engineering*, *71*, 106477. https://doi.org/10.1016/j.jobe.2023.106477

[51] Xiao, J., Lv, Z., Duan, Z., & Hou, S. (2022). Study on preparation and mechanical properties of 3D printed concrete with different aggregate combinations. *Journal of building engineering*, *51*, 104282. https://doi.org/10.1016/j.jobe.2022.104282

[52] Ye, J., Cui, C., Yu, J., Yu, K., & Xiao, J. (2021). Fresh and anisotropic-mechanical properties of 3D printable ultra-high ductile concrete with crumb rubber. *Composites part b: engineering*, *211*, 108639. https://doi.org/10.1016/j.compositesb.2021.108639

[53] Li, L. G., Xiao, B. F., Fang, Z. Q., Xiong, Z., Chu, S. H., & Kwan, A. K. H. (2021). Feasibility of glass/basalt fiber reinforced seawater coral sand mortar for 3D printing. *Additive manufacturing*, *37*, 101684. https://doi.org/10.1016/j.addma.2020.101684

[54] Zhou, J., Lai, J., Du, L., Wu, K., & Dong, S. (2022). Effect of directionally distributed steel fiber on static and dynamic properties of 3D printed cementitious composite. *Construction and building materials*, *318*, 125948. https://doi.org/10.1016/j.conbuildmat.2021.125948

[55] Pham, L., Tran, P., & Sanjayan, J. (2020). Steel fibres reinforced 3D printed concrete: Influence of fibre sizes on mechanical performance. *Construction and building materials*, *250*, 118785. https://doi.org/10.1016/j.conbuildmat.2020.118785

[56] Singh, A., Liu, Q., Xiao, J., & Lyu, Q. (2022). Mechanical and macrostructural properties of 3D printed concrete dosed with steel fibers under different loading direction. *Construction and building materials*, *323*, 126616. https://doi.org/10.1016/j.conbuildmat.2022.126616

[57] Arunothayan, A. R., Nematollahi, B., Ranade, R., Bong, S. H., Sanjayan, J. G., & Khayat, K. H. (2021). Fiber orientation effects on ultra-high performance concrete formed by 3D printing. *Cement and concrete research*, *143*, 106384. https://doi.org/10.1016/j.cemconres.2021.106384

[58] Hambach, M., Rutzen, M., & Volkmer, D. (2019). Properties of 3D-printed fiber-reinforced portland cement paste. In *3D concrete printing technology* (pp. 73–113). Butterworth-Heinemann. https://doi.org/10.1016/B978-0-12-815481-6.00005-1

[59] Ma, G., Li, Z., Wang, L., Wang, F., & Sanjayan, J. (2019). Mechanical anisotropy of aligned fiber reinforced composite for extrusion-based 3D printing. *Construction and building materials*, *202*, 770–783. https://doi.org/10.1016/j.conbuildmat.2019.01.008

[60] Li, L. G., Xiao, B. F., Cheng, C. M., Xie, H. Z., & Kwan, A. K. H. (2023). Adding glass fibers to 3D printable mortar: Effects on printability and material anisotropy. *Buildings*, *13*(9), 1–20. https://doi.org/10.3390/buildings13092295

[61] Panda, B., Chandra Paul, S., & Jen Tan, M. (2017). Anisotropic mechanical performance of 3D printed fiber reinforced sustainable construction material. *Materials letters*, *209*, 146–149. https://doi.org/10.1016/j.matlet.2017.07.123

[62] Chu, S. H., Li, L. G., & Kwan, A. K. H. (2021). Development of extrudable high strength fiber reinforced concrete incorporating nano calcium carbonate. *Additive manufacturing*, *37*, 101617. https://doi.org/10.1016/j.addma.2020.101617

[63] Hambach, M., Möller, H., Neumann, T., & Volkmer, D. (2016). Portland cement paste with aligned carbon fibers exhibiting exceptionally high flexural strength (> 100MPa). *Cement and concrete research*, *89*, 80–86. https://doi.org/10.1016/j.cemconres.2016.08.011

[64] Liu, B., Liu, X., Li, G., Geng, S., Li, Z., Weng, Y., & Qian, K. (2022). Study on anisotropy of 3D printing PVA fiber reinforced concrete using destructive and non-destructive testing methods. *Case studies in construction materials*, *17*, e01519. https://doi.org/10.1016/j.cscm.2022.e01519

[65] Sun, X., Zhou, J., Wang, Q., Shi, J., & Wang, H. (2022). PVA fibre reinforced high-strength cementitious composite for 3D printing: Mechanical properties and durability. *Additive manufacturing*, *49*, 102500. https://doi.org/10.1016/j.addma.2021.102500

[66] Zhao, Y., Wu, X., Zhu, L., Yang, Z., Wang, Y., & Xi, X. (2021). The influence of polypropylene fiber on the working performance and mechanical anisotropy of 3D printing concrete. *Journal of advanced concrete technology*, *19*(12), 1264–1274. https://doi.org/10.3151/jact.19.1264

[67] Zhang, Y., Zhu, Y., Ren, Q., He, B., Jiang, Z., Van Tittelboom, K., & De Schutter, G. (2023). Comparison of printability and mechanical properties of rigid and flexible fiber-reinforced 3D printed cement-based materials. *Construction and building materials*, *400*, 132750. https://doi.org/10.1016/j.conbuildmat.2023.132750